Nitrite Electroreduction Enhanced by Hybrid Compounds of Keggin Polyoxometalates and 1-Butyl-3-Vinylimidazolium

Yulin Zhou, Jing Sun, Sébastien Gallet, Jesus Raya, Corinne Boudon, Pierre-Antoine Bonnefont, Laurent Ruhlmann, Vasilica Badets

Research Article
doi.org/10.1002/cctc.202400226

Chemistry Europe
European Chemical Societies Publishing

www.chemcatchem.org

Nitrite Electroreduction Enhanced by Hybrid Compounds of Keggin Polyoxometalates and 1-Butyl-3-Vinylimidazolium

Yulin Zhou,[a, b] Jing Sun,[a, f] Sébastien Gallet,[c] Jesus Raya,[d] Corinne Boudon,[a] Antoine Bonnefont,[e] Laurent Ruhlmann,*[a] and Vasilica Badets*[a]

We describe here an immobilization method of four Keggin-type polyoxometalates (POMs) ($[H_2W_{12}O_{40}]^{6-}$, $[BW_{12}O_{40}]^{5-}$ $[SiW_{12}O_{40}]^{4-}$, $[PW_{12}O_{40}]^{3-}$) by using the reaction with an ionic liquid, 1-butyl-3-vinylimidazolium (BVIM) bromide. The reaction yields a hybrid material (BVIM-POM) as a water-insoluble salt. The chemical structure of both compounds is preserved, as indicated by infrared spectroscopy (FT-IR), although with a reduced crystallinity (shown by X-ray diffraction analysis) due to a decrease of water content (shown by thermogravimetric analysis). Cross polarization ^1H-^{31}P NMR evidenced the presence of BVIM in the structure of $(BVIM)_3[PW_{12}O_{40}]$. The salt is mixed with carbon powder and Nafion to prepare an ink and casted on glassy carbon electrodes. The electrochemical behavior of immobilized POMs material is preserved. The electrochemical activity for nitrite reduction is measured by cyclic voltammetry and differential electrochemical mass spectrometry (DEMS). It was observed that the reduction current of 10 mM HNO_2 at pH 1 in 0.5 M Na_2SO_4 is enhanced in the presence of these hybrid materials. DEMS has evidenced the formation of nitrous oxide (N_2O) at potentials more positive compared to the use of parent POMs in solution.

Introduction

Conversion of NO_x species (nitrate, nitrite/nitrous acid, nitric oxide, etc.) to harmless products such as nitrogen or useful chemicals such as ammonia and nitrous oxide is highly desirable to discard these environmental pollutants in an efficient manner. Amongst various techniques, electrochemical methods are quite clean as they require less external chemical adjuvants. In order to decrease the energy input, various electrochemical catalysts are investigated. One class of catalysts are the inorganic metal-oxides clusters named polyoxometalates (POMs). POMs can carry out reversible multi-electron transfer reactions without any change of their structure.[1] As reduction of NO_x species requires multiple electrons (equations 1–3), POMs are interesting candidates.

For these reasons, a large number of POMs with various structures were studied in literature, both as homogeneous and heterogeneous catalysts.[2–10] In our previous work, we have focused on the relationship between electrochemical properties of four POMs ($[H_2W_{12}O_{40}]^{6-}$, $[BW_{12}O_{40}]^{5-}$, $[SiW_{12}O_{40}]^{4-}$, $[PW_{12}O_{40}]^{3-}$) and the gaseous reaction products.[11] For this, we have employed the differential electrochemical mass spectrometry (DEMS) and POMs as homogeneous catalysts. Moreover, we have calculated the rate constant of the reaction between the reduced POM and HNO_2 and we have observed a direct relationship between the low anionic charge of the POM and the high rate constant. The selected compounds are W-based Keggin POMs with variable heteroatom. It must be noted that the total anionic charge can also be varied by replacing one W atom by one V or Mo atom, resulting in POMs stable even at neutral pH.[12,13] Nevertheless, our previous results, performed in aqueous solution at pH 1, showed that the studied POMs are promising catalyst for NO_x reduction and motivated the current research on the same POMs but as immobilized materials. The existing immobilization techniques are divided into the incorporation of POMs in various matrices and those based on the

$$NO_2^- + 2H_3O^+ + e^- \rightleftharpoons NO + 3H_2O \qquad E^0 = 1.202\ V/SHE \quad (eq.\ 1)$$

$$2NO_2^- + 6H_3O^+ + 4e^- \rightleftharpoons N_2O_{(g)} + 9H_2O \qquad E^0 = 1.396\ V/SHE \quad (eq.\ 2)$$

$$2NO_2^- + 8H_3O^+ + 6e^- \rightleftharpoons N_{2(g)} + 12H_2O \qquad E^0 = 1.520\ V/SHE \quad (eq.\ 3)$$

[a] Dr. Y. Zhou, Dr. J. Sun, Prof. C. Boudon, Prof. L. Ruhlmann, Dr. V. Badets
Laboratoire d'Electrochimie et de Chimie Physique du Corps Solide
Université de Strasbourg, Institut de Chimie, UMR CNRS 7177
4 Rue Blaise Pascal, CS 90032, 67081, Strasbourg Cedex, France
E-mail: lruhlmann@unistra.fr
badets@unistra.fr

[b] Dr. Y. Zhou
College of Chemical and Material Engineering
Quzhou University

[c] Dr. S. Gallet
IUT Robert Schuman, Université de Strasbourg
72 Route du Rhin, 67411 Illkirch-Graffenstaden, France

[d] Dr. J. Raya
Université de Strasbourg, Institut de Chimie, UMR CNRS 7177
4 Rue Blaise Pascal, CS 90032, 67081, Strasbourg Cedex, France

[e] Prof. A. Bonnefont
Univ. Grenoble Alpes, CNRS, Grenoble INP (Institute of Engineering, Univ. Grenoble Alpes), LEPMI F-38000 Grenoble, France

[f] Dr. J. Sun
Quzhou Baffil Chemical LLC (Quzhou Bafeier Huaxue LLC.)
Changshan Chemical Industrial Park
Changshan, Quzhou, Zhejiang, 324200, P.R. China

Supporting information for this article is available on the WWW under https://doi.org/10.1002/cctc.202400226

electrostatic interaction, benefiting from the inherent anionic charge. Examples of matrices are: gelatin for $[BW_{12}O_{40}]^{5-}$,[14] QPVP matrices (poly(4-vinylpyridine cross linked with 1,12-dibromododecane) for $[SiW_{12}O_{40}]^{4-}$,[15] carbon paste electrode for $[SiW_{12}O_{40}]^{4-}$.[16] Examples based on electrostatic interaction are organic inorganic hybrid structures for $[BW_{12}O_{40}]^{5-}$ and $[PW_{12}O_{40}]^{3-}$,[17,18] and metal-organic frameworks for $[H_2W_{12}O_{40}]^{6-}$.[19,20]

Ionic liquids are currently used in electroanalysis due to their good conductivity and tunable solvent properties. Indeed, the reaction between POMs and ionic liquid has been proposed for several examples,[21–23] but only few examples, such as the Mo-based Keggin POM ($[PMo_{12}O_{40}]^{3-}$ and $[BW_{12}O_{40}]^{5-}$ were used in development of sensors for nitrite reduction.[14] As ionic liquid, the following compounds were tested: 1-n-Butyl-3-methylimidazolium tetrafluoroborate ($BMIMBF_4$),[24,25] 1-mehtyl-3-methylimidazolium tetrafluoroborate ($EMIMBF_4$), their bromide analogues,[26] and N-dodecyl pyridinium hexafluorophosphate ($[C_{12}Py]PF_6$]).[27] When used as binder in the construction of a carbon paste electrode, the ionic liquid contributed to the enhancement of conductivity and behaved as a charge-transfer bridge, facilitating the electrons intake from the POM.[24,25] It was also shown that the hydrophobic alkyl chain of ($[C_{12}Py]PF_6$]) strongly interacts with the carbon nanotubes, thus reducing the charge transfer resistance between the immobilized POM and the electrode.[27]

In our work, we have chosen alternative ionic liquid, 1-butyl-3-vinylimidazolium (BVIM) bromide, for its ability to polymerize. Indeed, using a radical polymerization of the vinyl group, a polymerized ionic liquid (PIL) containing onium cations fixed on the main chain is obtained.[28] This PIL was used for immobilization of glucose oxidase[29] and hemoglobin,[30] based on self-assembly between positive groups of the polymer and negative groups of the biological macromolecule. In fact, we have conducted preliminary work to immobilize our POMs by using this PIL (and reduced graphene oxide). Nevertheless, the obtained electrodes suffered from a very high capacitive current and high charge transfer resistance, mostly due to a dramatic decrease of the ionic conductivity of the PIL. This phenomenon is well documented[26] and it is ascribed to the reduced number of mobile ions and to an important increase of glass transition temperature. Based on this, we have decided to immobilize our POMs by using the simple and direct reaction with BVIMBr, in which the exchange of POMs inherent cation (Na^+, K^+, NH_4^+) with the imidazolium cation leads to an insoluble salt. The main interest is to reduce the solubility of POMs for assuring a stable immobilization at the electrode surface, while preserving the electrochemical behavior.

Results and Discussion

Preparation and Characterization of BVIM-POMs

The preparation of BVIM-POM salt consists in the chemical reaction between parent POM and BVIMBr in aqueous phase, as these compounds are soluble in water. The cation exchange leads to a water-insoluble salt of white color. The principle is detailed in Scheme 1 with starting POM $[SiW_{12}O_{40}]^{4-}$ as an example. As described in the experimental part, the parent POMs were dissolved in water (pH 6.5). In POMs chemistry, one should consider the stability of each chosen compound in function of pH.

While $[H_2W_{12}O_{40}]^{6-}$ and $[BW_{12}O_{40}]^{5-}$ are stable up to pH 7,[31] $[SiW_{12}O_{40}]^{4-}$ is stable up to pH 5 and $[PW_{12}O_{40}]^{3-}$ only up to pH 1.7.[32] In fact, the stability of $[SiW_{12}O_{40}]^{4-}$ and of $[PW_{12}O_{40}]^{3-}$ (amongst other POMs) was thoroughly studied using ^{31}P and ^{183}W NMR for these compounds dissolved in various buffers at various pHs (Hepes buffer pH 7.5 for $[SiW_{12}O_{40}]^{4-}$ and acetate buffer at pH 5.5 for $[PW_{12}O_{40}]^{3-}$).[13] In these conditions, a mixture of initial POM and the isomer obtained after removal of one {WO} unit is obtained.[13] In our conditions, after the addition of each POM in water, the pH became 4.29 for $[H_2W_{12}O_{40}]^{6-}$, 4.43 for $[BW_{12}O_{40}]^{5-}$, 4.43 for $[SiW_{12}O_{40}]^{4-}$ and 1.77 for $[PW_{12}O_{40}]^{3-}$. Thus, especially for $[PW_{12}O_{40}]^{3-}$, the existence of some isomers in the final hybrid compound is not excluded. In the case of $[BW_{12}O_{40}]^{5-}$, one could discuss about the possible formation of $[BW_{12}O_{40}]^{5-}$, but this was not evidenced by hydrolysis experiments in the pH range 7 to 10. Moreover, the conversion between $[BW_{11}O_{39}]^{8-}$, $[BW_{13}O_{46}H_3]^{8-}$ and $[B_3W_{39}O_{132}]^{21-}$ is rapid and reversible, but the starting compound is not $[BW_{12}O_{40}]^{5-}$, but rather $B(OH)_3$ and WO_4^{2-}.[31] The electro-

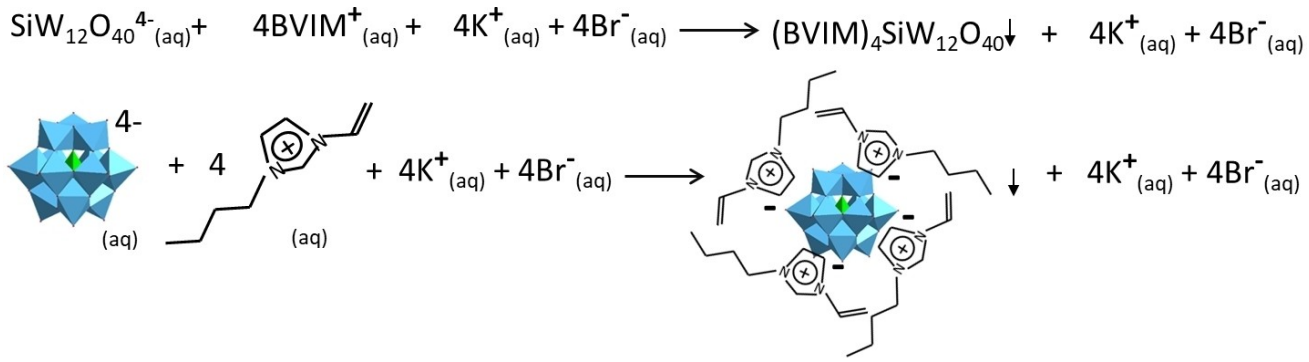

Scheme 1. Reaction between starting POM $[SiW_{12}O_{40}]^{4-}$ and ionic liquid 1-butyl-3-vinylimidazolium (BVIM) bromide in aqueous phase leading to insoluble $(BVIM)_4[SiW_{12}O_{40}]$.

Table 1. Elemental analysis of BVIM-POMs hybrid compounds.

Compound	% C calculated (found)	% H calculated (found)	% N calculated (found)
$(BVIM)_6[H_2W_{12}O_{40}]$	17.3 (17.1)	2.4 (2.5)	4.5 (4.0)
$(BVIM)_5[BW_{12}O_{40}]$	14.9 (14.9)	2.1 (2.1)	3.9 (3.6)
$(BVIM)_4[SiW_{12}O_{40}]$	12.4 (12.3)	1.7 (1.8)	3.2 (2.7)
$(BVIM)_3[PW_{12}O_{40}]$	9.7 (9.8)	1.4 (1.4)	2.5 (2.2)

chemical behavior is an easy tool to distinguish between the $[BW_{12}O_{40}]^{5-}$ and $[BW_{11}O_{39}]^{8-}$.[31]

CHNS elemental analysis was used to compute the percentage of C and N and H in the final BVIM-POM salts. For all four salts the values correspond to the complete replacement of initial cations by the BVIM (Table 1). Thus, the final composition is $(BVIM)_6[H_2W_{12}O_{40}]$, $(BVIM)_5[BW_{12}O_{40}]$, $(BVIM)_4[SiW_{12}O_{40}]$, and $(BVIM)_3[PW_{12}O_{40}]$. Nevertheless, for $(BVIM)_3[PW_{12}O_{40}]$ the CHN analysis could as well indicate the formation of $Na_4(BVIM)_3PW_{11}O_{39}$, due to a possible existence of $PW_{11}O_{39}^{7-}$ isomer when $[PW_{12}O_{40}]^{3-}$ is dissolved in water (calculated % C 10.1, % H 1.4, % N 2.6) (vide supra). For this reason, the phosphorous based hybrid compound is denoted "$(BVIM)_3[PW_{12}O_{40}]$".

FT-IR spectrum of the 1-butyl-3-vinylimidazolium bromide (BVIMBr) alone is shown in Figure 1 (red curve). The characteristic bands of imidazolium ring are: C–H in imidazole ring stretching between 3023–3130 cm^{-1}; imidazole ring stretching 1567, 1543, 1465 cm^{-1}; H–C–C and H–C–N in imidazole ring bending 1165 cm^{-1}; in-plane imidazole ring bending 881 cm^{-1}; out of plane C–H bending of imidazolium ring 738 cm^{-1}; imidazolium C–N–C 657 cm^{-1}.

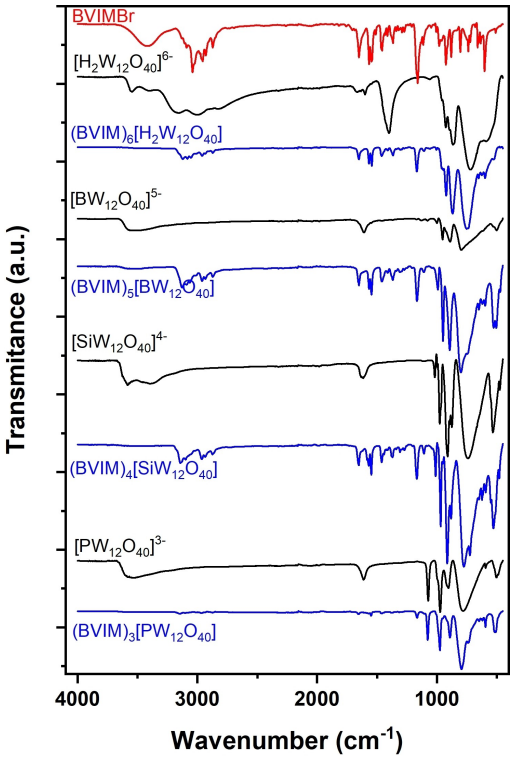

Figure 1. FT-IR spectra of BVIMBr (red curve), parents POMs (black curves) and BVIM-POM hybrid materials (blue curves).

Our BVIMBr contains a vinyl group for which the characteristic band are observed at 1652 cm^{-1} (C=C stretching) and in similar range as the C–H stretching of imidazolium ring. FT-IR spectra of the parent POMs are displayed in Figure 1 (black curves). The characteristic bands of $[H_2W_{12}O_{40}]^{6-}$ cluster are: $W–O_{terminal}$ stretching 927 cm^{-1}; corner sharing W–O–W stretching 860 cm^{-1}; edge sharing W–O–W stretching 720 cm^{-1}. For $(NH_4)_6[H_2W_{12}O_{40}]$, the N–H stretching in ammonium group is visible at 1400 cm^{-1}. A strong adsorption band corresponding to O–H bending at ~1610 cm^{-1} is visible for $[PW_{12}O_{40}]^{3-}$, $[SiW_{12}O_{40}]^{4-}$ and $[BW_{12}O_{40}]^{5-}$ and less visible for $[H_2W_{12}O_{40}]^{6-}$ (this compound contains less crystalline water).

Actually, the constitution water molecules were determined from TGA analysis (vide infra). FT-IR spectra of the hybrid materials (Figure 1 blue curves) prove that the structure of both 1-butyl-3-vinylimidazolium cation and the POM anion are preserved because several characteristic bands of both POMs and $BVIM^+$ are visible: C–H stretching in vinyl and imidazolium ring at 3052, 3083, 3121 cm^{-1}, ring stretching 1567, 1543, 1465 cm^{-1}; C=C stretching of vinyl group at 1652 cm^{-1}; imidazole H–C–C and H–C–N bending 1159–1171 cm^{-1}; $W–O_{terminal}$ stretching 923 cm^{-1}; edge sharing W–O–W stretching 867 cm^{-1}; corner sharing W–O–W stretching 753 cm^{-1}. A complete list of all vibration recorded in the FT-IR spectra is given in Table S1, Table S2 and Figure S1.[33–35]

In the case of "$(BVIM)_3[PW_{12}O_{40}]$", no band characteristic to a free phosphate unit $\{PO_4\}$[36] or to $[PW_{11}O_{39}]^{7-}$[22] that could come from the decomposition of $[PW_{12}O_{40}]^{3-}$ when dissolved in water is observed. Control experiments were performed by mixing a solution of NaH_2PO_4 prepared in water (30 mM) with an aqueous solution of BVIMBr (60 mM), but no precipitation was observed. Similarly, when 30 mM of Na_2WO_4 was treated with 120 mM of BVIMBr, no precipitation was observed. This suggests that, even if some decomposition of $[PW_{12}O_{40}]^{3-}$ occurs, some of the resulting anions are not included in the final hybrid compound.

Interestingly, the water content of hybrid materials is reduced in a POM dependent manner. For example, for $(BVIM)_6[H_2W_{12}O_{40}]$ and $(BVIM)_4[SiW_{12}O_{40}]$ the large band at 3400 cm^{-1} (–OH stretching of H_2O) disappeared almost completely. This phenomenon was observed for other POM-ionic liquid hybrid materials, such as the one resulting from pairing

$[H_4PW_{18}O_{62}]^{7-}$ or $[P_2W_{18}O_{60}]^{6-}$ with 1-butyl-3-methylimidazolium $[BMIM]^+$ cation.[21] But for $(BVIM)_5[BW_{12}O_{40}]$ and "$(BVIM)_3[PW_{12}O_{40}]$" a slight quantity of water is still present, especially in the second compound (Figure S2). It can be noted that parent POMs of these two compounds initially contain a higher number of constitution water molecules as determined from TG analysis.

The thermogravimetric behavior of BVIM, parent POMs and hybrid materials is displayed in Figure 2a and Figures S3–S5. The TGA curve of BVIMBr shows a total weight loss starting at 300 °C and completing at 600 °C. This is attributed to the decomposition of ionic liquid. Thermal analysis of all parent POMs shows an initial mass loss from about 100 °C to 300 °C corresponding to the water loss since all POMs contain constitution water molecules. Besides, this analysis gives the possibility to compute exactly how many water molecules are present. Thus, we obtain $(NH_4)_6[H_2W_{12}O_{40}]*4H_2O$, $K_5[BW_{12}O_{40}]*7H_2O$, $K_4[SiW_{12}O_{40}]*4H_2O$ and $Na_3[PW_{12}O_{40}]*12H_2O$ in the case of the parent POMs (Figure S2). Thus, the water loss is accounted for 2%, 4%, 3% and 7% respectively. Above 300 °C a slight slow decomposition of POMs is observed, except for $(NH_4)_6[H_2W_{12}O_{40}]*3H_2O$ for which a clear decomposition from 300 to 400 °C, accounting for 4% of mass loss, is observed (Figure S3). This is probably associated to the decomposition of accompanying ammonium cation happening before the decomposition of the Keggin anion.

For all hybrid materials, the thermal stability is improved as only 1% mass loss is observed up to 300 °C (Figure 2a). This is explained by the fact that almost no water is available in the hybrid materials. This corroborates with the FT-IR spectra that show a clear decrease in the water content (vide supra). Above 300 °C, significant weight losses of about 24%, 20%, 16% and 13% for $(BVIM)_6[H_2W_{12}O_{40}]$, $(BVIM)_5[BW_{12}O_{40}]$, $(BVIM)_4[SiW_{12}O_{40}]$ and "$(BVIM)_3[PW_{12}O_{40}]$" are observed for the hybrid materials. This is associated with the decomposition of the organic cation and corresponds to the theoretical percentage of the cation in the BVIM-POM materials. DSC analysis of ionic liquid, hybrid materials and parent POMs is shown in Figure 2b and Figures S3–S5. In Figure 2b, data are stacked for better comparison. Detailed values of heat flow and TGA coupled analysis can be found in Figures S3–S5. It can be observed that the fusion of BVIMBr appears at T_{onset} of 82.33 °C (very sharp endothermic peak), followed by its combustion at T_{onset} of 214.82 °C (small exothermic peak). After this temperature, the heat flow is erratic, as the combustion produces some effervescence. The fusion of hybrid materials is POM-dependent, with no clear correlation between the equivalents of hybrid cation ($BVIM^+$) and the fusion temperature. Precisely, a very sharp endothermic peak appears at T_{onset} of 123.32 °C, 72.34 °C, 217.96 °C and 179.67 °C for $(BVIM)_6[H_2W_{12}O_{40}]$, $(BVIM)_5[BW_{12}O_{40}]$, $(BVIM)_4[SiW_{12}O_{40}]$ and "$(BVIM)_3[PW_{12}O_{40}]$" respectively. The combustion appears at T_{onset} of 253.16 °C, 249.45 °C, 248.88 °C and 310.83 °C for $(BVIM)_6[H_2W_{12}O_{40}]$, $(BVIM)_5[BW_{12}O_{40}]$, $(BVIM)_4[SiW_{12}O_{40}]$ and "$(BVIM)_3[PW_{12}O_{40}]$" respectively. The combustion appears as an exothermic peak and after this, the heat flow is erratic, as the combustion produces some effervescence, as in the case of BVIMBr alone.

The powder X-ray diffraction pattern of parent POMs and hybrid materials are shown in Figure S6. The results show that pure Keggin salts have a better defined structured compared to hybrid BVIM-POM materials. This can be explained by the changes in the secondary structure of the POMs induced by the ionic liquid. These changes are explained by the removal of constitution water molecules but also by the fully replacement of small cations (NH_4^+, K^+, Na^+) with a bulkier cation ($BVIM^+$). A similar behavior was observed for other examples of hybrid materials, such as the ones obtained from Dawson-type POMs $K_7[H_4PW_{18}O_{62}]$ and $K_6[P_2W_{18}O_{62}]$ and 1-butyl-3-methylimidazolium tetrafluoroborate.[21] Particularly for "$(BVIM)_3[PW_{12}O_{40}]$" the crystalline structure is completely amorphous. For a further confirmation about the molecular structure of this compound, solid ^{31}P NMR measurements were performed for parent POM $Na_3[PW_{12}O_{40}]$ and hybrid material "$(BVIM)_3[PW_{12}O_{40}]$". In Figure 3a, the signals of ^{31}P atom at −16.26 ppm and at −16.19 ppm (slightly wider) respectively are observed. In Figure 3b, the interaction between the protons of BVIM with phosphorus atom is obvious for the hybrid material (black curve), while it is missing for the parent POM (red curve), as expected.

It is worthy to note that, in Figure 3a, the black curve of "$(BVIM)_3[PW_{12}O_{40}]$" displays only one peak. This suggests that

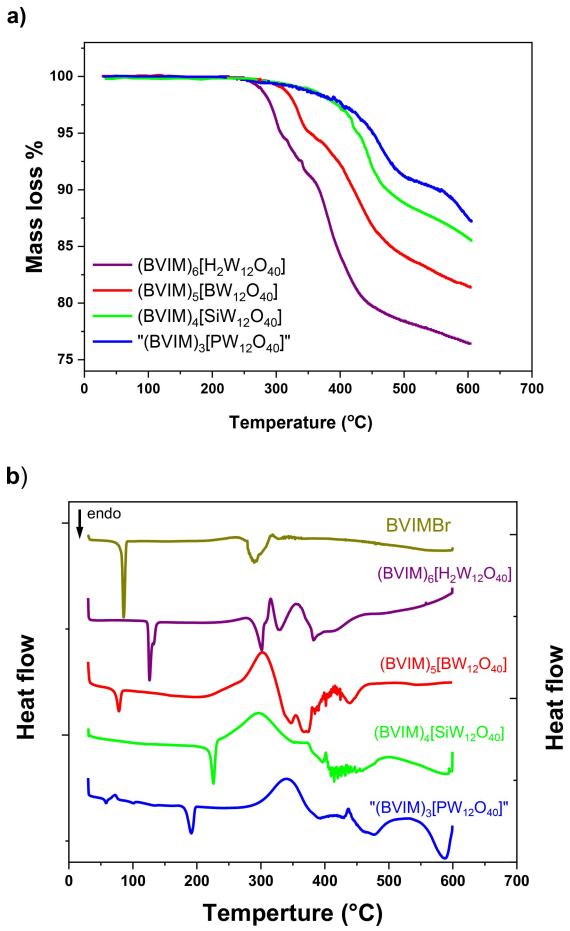

Figure 2. a) TG and b) DSC analysis of BVIM-POM hybrid materials.

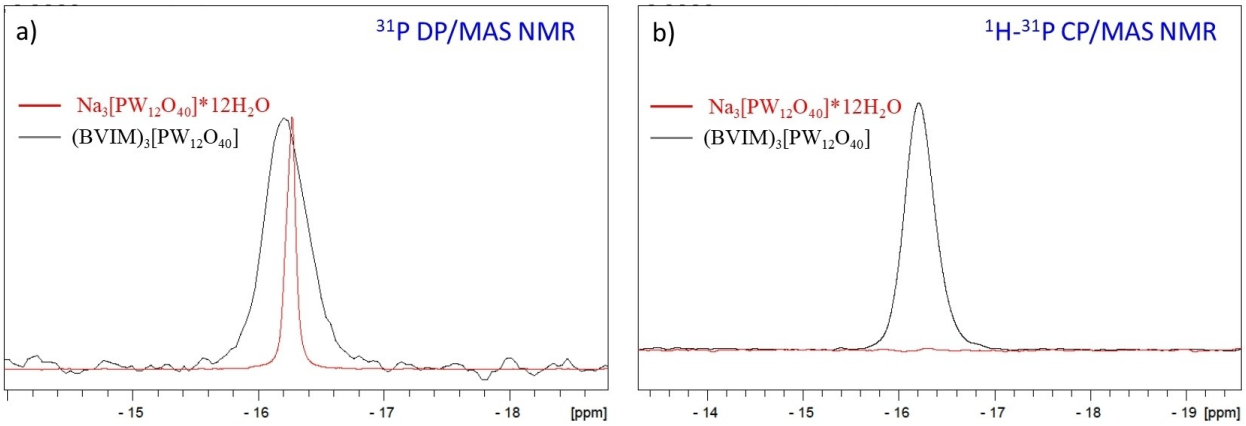

Figure 3. a) Solid ^{31}P NMR spectra of parent POM ($Na_3[PW_{12}O_{40}]$) and $(BVIM)_3[PW_{12}O_{40}]$ hybrid material and (b) cross polarization ^{1}H-^{31}P NMR spectra.

there is only one type of phosphorus atom and discard the hypothesis of having a solid mixture of "$(BVIM)_3[PW_{12}O_{40}]$" and of $Na_4(BVIM)_3PW_{11}O_{39}$.

Electrochemical Behavior of Immobilized BVIM-POMs

After the immobilization of BVIM-POM hybrid materials on glassy carbon electrode, it is essential to observe the number of redox peaks and, if possible, the number of exchanged electrons. Figure 4 shows the cyclic voltammetry of immobilized BVIM-POMs (blue curves) in comparison with parent POMs in solution (black curves). All the peaks are symmetric, as specific

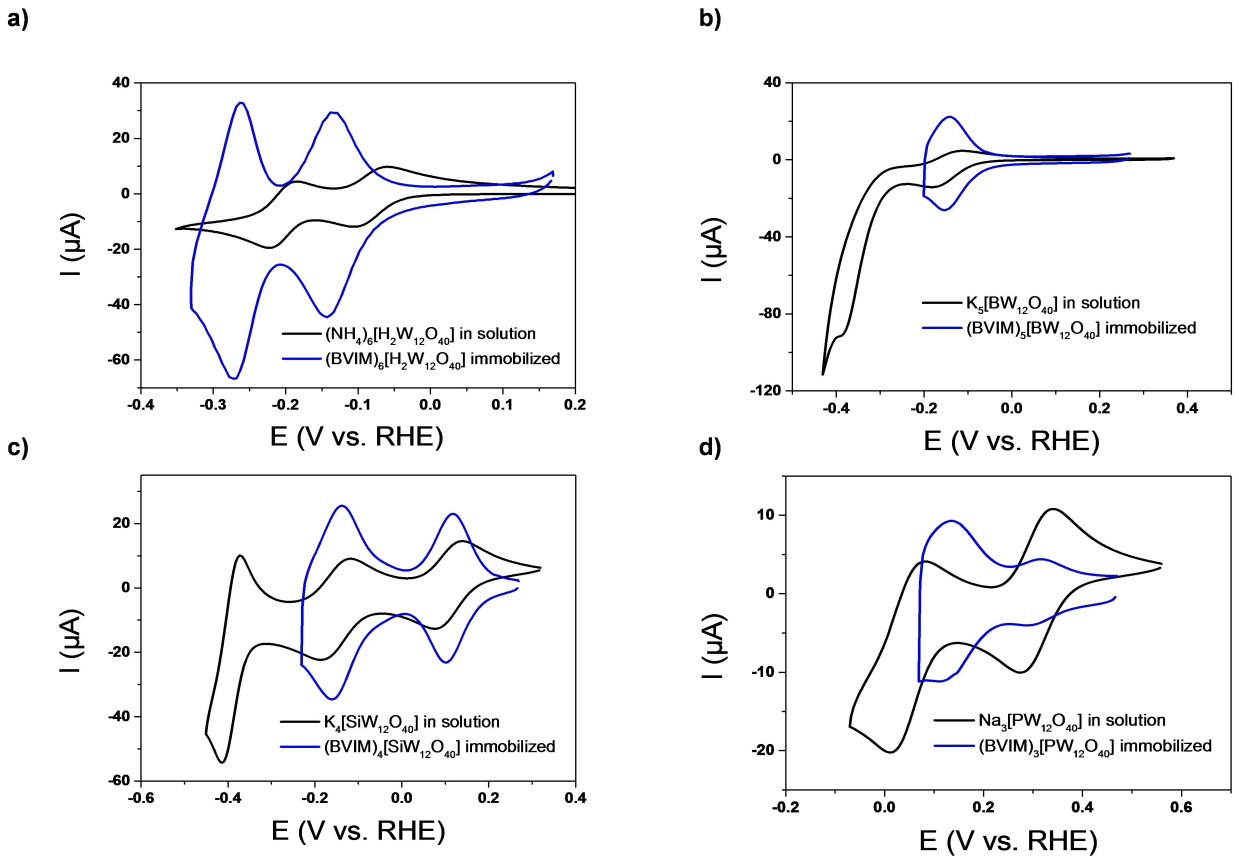

Figure 4. Cyclic voltammetry of immobilized hybrid BVIM-POM (blue line) compared to parent POM in solution (black line): a) $(BVIM)_6[H_2W_{12}O_{40}]$, b) $(BVIM)_5[BW_{12}O_{40}]$, c) $(BVIM)_4[SiW_{12}O_{40}]$, d) $(BVIM)_3[PW_{12}O_{40}]$. Experimental conditions: scan rate, 20 mVs^{-1}; electrolyte, 0.5 M Na_2SO_4, pH 1; 1 mM POM (only for CV with POM in solution, black line).

Table 2. Electrochemical parameters if immobilized BVIM-POMs hybrid compounds.

Compound	ΔE (V) Ist wave	ΔE (V) IInd wave	Surface coverage (Γ/mol cm^{-2})	$E^{0'}$ of POMs in solution[a] (V *vs.* RHE)	$E^{0'}$ of immobilized BVIM-POMs[b] (V *vs.* RHE)	Peak shift ($E^{0'}_{immobilized}$-$E^{0'}_{sn\ solution}$) (V)
$(BVIM)_6[H_2W_{12}O_{40}]$	0.007	0.009	5.8*10−8	−0.084	−0.140	−0.056
$(BVIM)_5[BW_{12}O_{40}]$	0.009	n.d.	6.8*10−8	−0.128	−0.159	−0.031
$(BVIM)_4[SiW_{12}O_{40}]$	0.017	0.020	7.2*10−8	0.132	0.099	−0.033
$(BVIM)_3[PW_{12}O_{40}]$	0.023	0.019	1.3*10−8	0.291	0.305	0.014

[a] from our previous work[11] and only for the Ist wave. [b] this work and only for the Ist wave where $E^{0'} = (E_{pa} + E_{pc})/2$.

to an immobilized redox species. For $(BVIM)_6[H_2W_{12}O_{40}]$ two pairs of peaks, with similar current intensities, are observed (Figure 3a). This is similar to parent $(NH_4)_6[H_2W_{12}O_{40}]$, suggesting that each peak corresponds to two exchanged electrons. For $(BVIM)_5[BW_{12}O_{40}]$, only one pair of peaks is observed. The potential was not scanned to lower values because this leads to a degradation of the first pair of peaks. The parent $K_5[BW_{12}O_{40}]$ displays one electron wave followed by a five electrons wave at much lower potentials, as expected for this compound,[32] confirming the absence of any other $[BW_{11}O_{39}]^{8-}$ in the starting material. This is the case also for $(BVIM)_5[BW_{12}O_{40}]$. For $(BVIM)_4[SiW_{12}O_{40}]$, two pairs of peaks, with similar current intensities, are observed. This is similar to parent $K_4[SiW_{12}O_{40}]$, suggesting that each peak corresponds to one exchanged electron. The third pair of peaks could again not be observed because potential was not scanned to lower values to avoid a degradation of the first two pairs of peaks. Finally, for "$(BVIM)_3[PW_{12}O_{40}]$" two pairs of peaks are observed but with different current intensities (the first pair is smaller than the second one). It thus must be noted the peculiar redox behavior of the immobilized "$(BVIM)_3[PW_{12}O_{40}]$" (vide infra). This is different from the parent POM that present two pairs of peaks with similar intensity, corresponding to one exchanged electron.

The redox behavior of immobilized hybrid BVIM-POMs is also analyzed by measuring the peak-to-peak separation (ΔE) (Table 2). For $(BVIM)_6[H_2W_{12}O_{40}]$ and $(BVIM)_5[BW_{12}O_{40}]$ values closed to zero are obtained, showing a fully reversible immobilized redox system. For the other two hybrid POMs, values are around 0.020 V, suggesting a small deviation from the reversible behavior or a diffusion of the compounds into the immobilization matrix. The surface coverage (Γ/mol cm^{-2}) of immobilized BVIM-POMs was calculated from the total charge (Q) exchanged during the first cathodic wave (by computing the area of this peak) (Table 2). Very similar values were obtained for three BVIM-POMs, while the amount of immobilized "$(BVIM)_3[PW_{12}O_{40}]$" is smaller. A comparison between the redox behavior of hybrid BVIM-POM immobilized on glassy carbon electrode and the parent POMs dissolved in solution is also made via the formal peak potential, E°′, computed as the average of anodic (E_{pa}) and cathodic peak (E_{pc}). The values are listed in Table 2. A slight negative shift is observed for almost all BVIM-POMs that may be related to a local small pH increase or to an existing junction potential at the interface of immobilized film and the solution. For "$(BVIM)_3[PW_{12}O_{40}]$" a slight positive shift is observed. This indicates one more time the special redox behavior of this immobilized POM that could be tentatively explained by the existence of a mixture between "$(BVIM)_3[PW_{12}O_{40}]$" and $Na_4(BVIM)_3PW_{11}O_{39}$, although the lacunary compound should display its redox waves at more negative potential.

Electrochemical Reduction of Nitrite

The immobilization of POMs is a necessary condition for a heterogeneous catalysis and the choice of immobilization matrix is important for preserving the redox activity. One should inquire about the participation of the immobilization material itself at the catalytic activity. For this reason, we have firstly studied nitrite reduction at a glassy carbon electrode modified with carbon black ink, because this represents the immobilization matrix of our hybrid BVIM-POMs. Figure 5 shows the cyclic voltammetry results obtained with a GC/C electrode and various concentrations of nitrite in solution. The reduction current starts to increase at the beginning of the measurements, at 0.8 V *vs.* RHE. Also, the reduction current increases along with nitrite concentration. In this case, one should not neglect the role played by the immobilization material. Next, we have immobilized our hybrid BVIM-POMs on the GC/C and measure whether the nitrite reduction is enhanced. Firstly, we have used cyclic voltammetry measurements. Figure 6 shows the CVs before

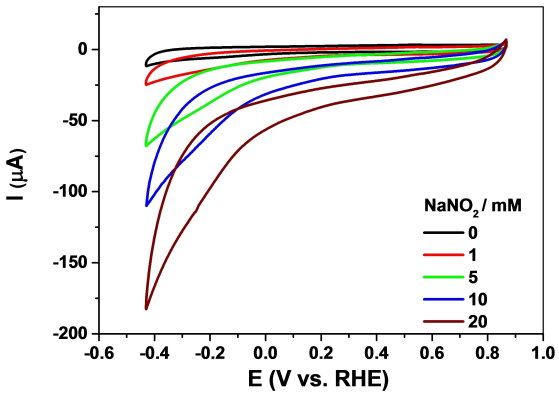

Figure 5. Cyclic voltammetry analysis of nitrite reduction with GC/C electrode. Experimental conditions: electrolyte, 0.5 M Na_2SO_4, pH 1; scan rate, 0.5 mVs^{-1}; 10 mM $Na^{15}NO_2$.

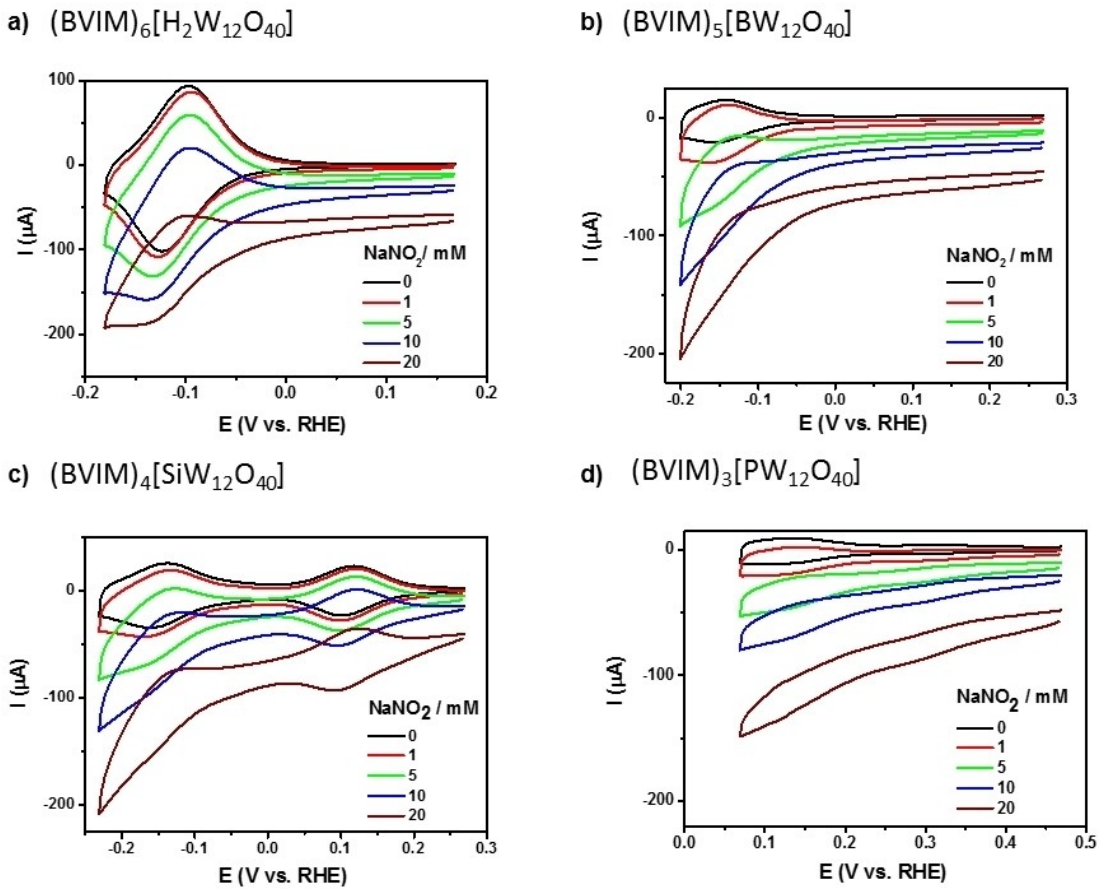

Figure 6. Cyclic voltammetry analysis of nitrite reduction with immobilized BVIM-POM hybrid materials. Experimental conditions: electrolyte, 0.5 M Na_2SO_4, pH 1; scan rate, 0.5 mVs^{-1}; 10 mM $Na^{15}NO_2$.

addition of nitrite (black curve), followed by subsequent additions of $NaNO_2$, from 1 to 20 mM. An increase of the reduction current is observed each time on the entire potential range. Also, irrespective of the used BVIM-POM, one should notice the reduction current observed at the beginning of the scan, before the reduction peak of BVIM-POMs. As described just before, this is due to the nitrite reduction on the GC/C electrode alone. It should be noted that a similar situation was described for the immobilization of another POM, $[SiMo_{12}O_{40}]^{4-}$ in a polyaniline (PANI) matrix. Precisely, a reduction current for nitrite reduction was recorded at 0.8 V *vs.* RHE at the modified GC/PANI/POM, while the reduction peak of POM appears only at 0.45 V *vs.* RHE.[15]

One should observe the advantage brought by the use of BVIM-POM hybrid materials. In Figure 7, the comparison of linear sweep voltammetry (obtained during the DEMS analysis described below) shows that the reduction current of nitrite is almost 2 times higher at the GC/C/BVIM-POMs compared to GC/C and GC electrode (measured at −0.2 V for almost materials and at 0 V *vs.* RHE for "$(BVIM)_3[PW_{12}O_{40}]$").

For a better characterization of BVIM-POM activity towards nitrite reduction, differential electrochemical spectroscopy was used. The purpose is to find the gaseous products and understand the contribution of GC/C electrode and BVIM-POM to nitrite reduction.

We have found that on GC/C electrode there is no formation of NO and the onset potential of N_2O is around 0.05 V *vs.* RHE (Figure S7). For all four BVIM-POMs, also no formation of NO was observed and, after a stable zero baseline, the signal decreases (Figure 8). Moreover, this decrease is very well correlated with the increase of the N_2O signal. The explanation for this is that NO is consumed to produce N_2O. The source of NO is most probably the disproportionation of HNO_2 (eq. 4).[37] This behavior is completely different with the case of POMs in solution, where a formation of NO, from the catalyzed reduction of HNO_2, is observed. One possible explanation is that the diffusion of NO away from the electrode surface into the bulk of the solution is much slower than its subsequent conversion to N_2O (eqs. 5–7). Thus, the amount of NO available in solution is below the detection limit of the DEMS. At this stage, we can compare our results with the only published paper so far, that is the nitrite reduction catalyzed by $H_4[SiMo_{12}O_{40}]$ immobilized in a poly-pyrrole matrix on a platinum electrode.[38] In that case, DEMS analysis showed the consumption of NO and the formation of N_2O, similar to our case.

A second observation is the dependence of N_2O onset potential on the charge of POM (Figure 9), although the values

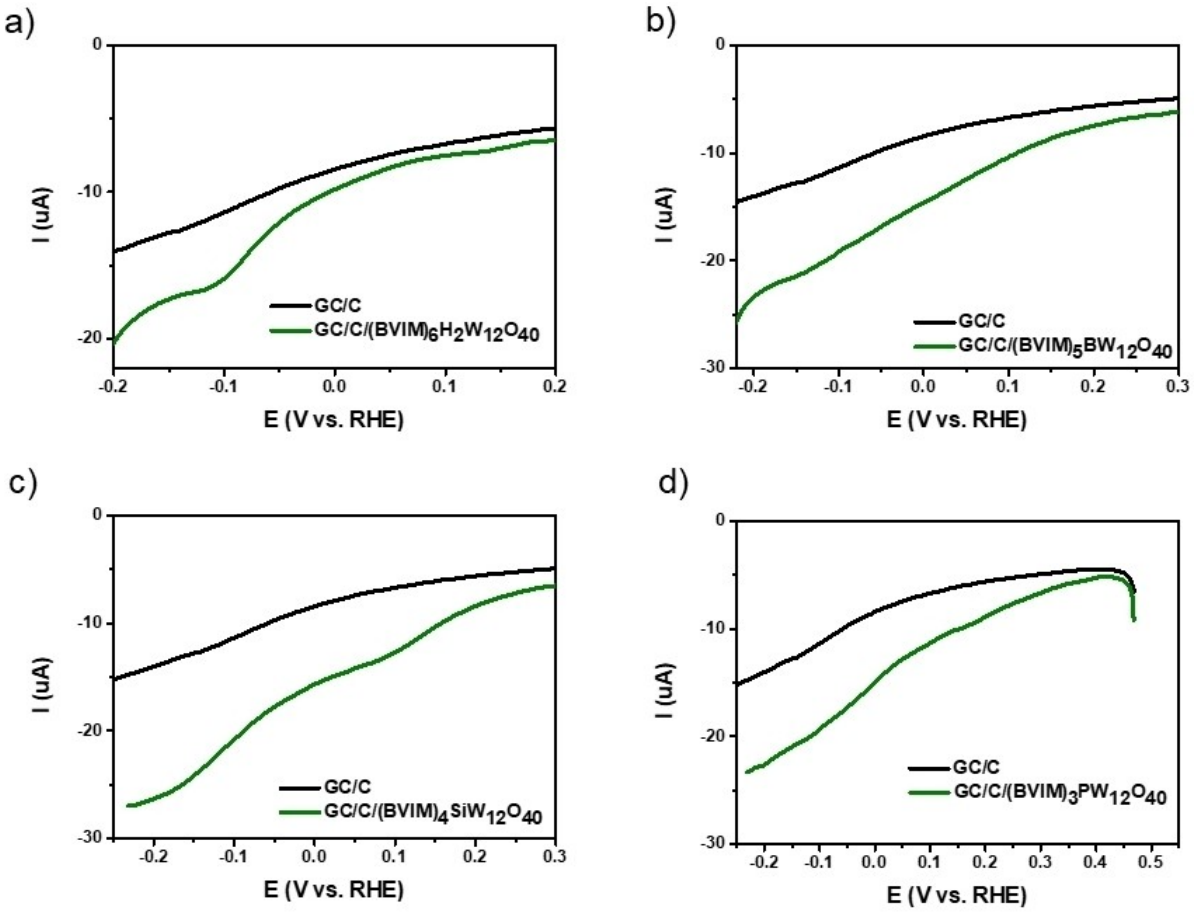

Figure 7. Comparisons of linear sweep voltammetry of nitric acid reduction with glassy carbon electrode modified with carbon black (GC/C) and glassy carbon electrode modified with carbon black and BVIM-POM hybrid materials (GC/C/BVIM-POM). Experimental conditions: electrolyte, 0.5 M Na_2SO_4, pH 1; scan rate, 0.5 mVs^{-1}; 10 mM $Na^{15}NO_2$.

belong to a narrow range between 0.10 and 0.15 V *vs.* RHE. These values are quite more positive than those obtained with respective POMs in solution. This excludes the mechanism of N_2O formation via an HNO intermediate, as described in our previous paper (eq. 5).[11] Another mechanism can be proposed, based on the reaction between one adsorbed molecule of NO and one molecule of NO in the solution phase, leading to the HN_2O_2(ads) dimer (eqs. 6–7).[39] But it is also difficult to assume this mechanism because of the improbability of having NO adsorbed on a carbonaceous material. One may consider the adsorption of NO on the polyoxometalates. In fact, this is happening at high temperature.[40,41] It was suggested that nitric oxide is trapped as $H_2NO_2^+$ and replaces the $H_5O_2^+$ species in the crystalline structure. In our case, when the immobilized POM is reduced, its overall negative charge increases. The charge balance could be achieved by some $H_5O_2^+$. Hence the adsorption of nitric oxide could be facilitated. But, at this stage the mechanism remains unknown and other spectroscopic techniques (such as *in situ* infrared spectroscopy) and computational modelling are required in order to clarify it.[41,42]

$$3HNO_2 \rightarrow 2NO(aq) + HNO_3 + H_2O \quad \text{(eq. 4)}$$

$$2NO(aq) + 2H^+ + 2e^- \rightarrow 2HNO(aq) \rightarrow N_2O(aq) + H_2O \quad \text{(eq. 5)}$$

$$NO(ads) + NO(aq) + H^+ + e^- \rightarrow HN_2O_2(ads) \quad \text{(eq. 6)}$$

$$HN_2O_2(ads) + H^+ + e^- \rightarrow N_2O(aq) + H_2O \quad \text{(eq. 7)}$$

Conclusions

We have described the synthesis and electrochemical properties of new hybrid materials obtained by the reaction of four Keggin-type POMs with the ionic liquid, 1-butyl-3-vinyl-imidazolium bromide (BVIM). Several physico-chemical characterization techniques (FT-IR, TGA, DSC, XRD, solid ^{31}P-NMR) have been used to show that POMs preserve their structure in the hybrid materials, although with a reduced water content and reduced crystallinity. The redox behavior of immobilized hybrid BVIM-POM is similar to parent compounds, with the exception of "$(BVIM)_3PW_{12}O_{40}$" for which a shift to more positive potentials was observed. The hybrid materials contribute to the increase of the current of nitrite reduction, although a different mechanism is supposed. This is sustained by DEMS analysis from which a very positive onset of N_2O formation was observed. It was also found that carbon ink displays an

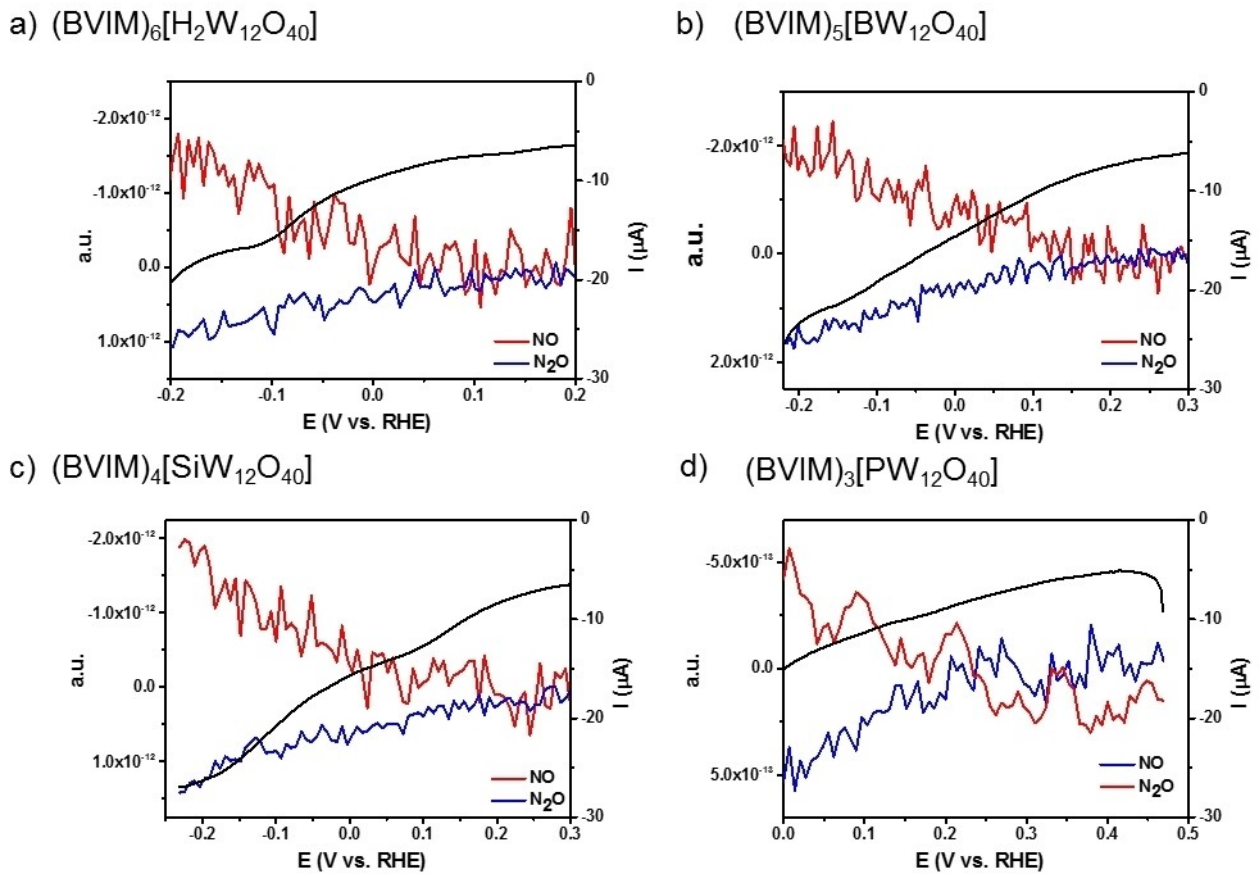

Figure 8. DEMS analysis of nitrite reduction with immobilized BVIM-POMs. Experimental conditions: electrolyte, 0.5 M Na_2SO_4, pH 1; scan rate, 0.5 mVs^{-1}; 10 mM $Na^{15}NO_2$.

unexpected activity because the N_2O onset was also observed at more positive potential when compared to glassy carbon alone. For better understanding the mechanism and elucidate if the nitric oxide absorbs on these materials, *in situ* infrared spectroscopy and computational modelling should be used in the future. Also, a higher variety of the ionic liquids should be tested in order to fully describe the influence of such compounds on the efficiency of the immobilization and on nitrite electroreduction.

In conclusion, we have shown that the immobilization of several POMs using an ionic liquid preserves their activity for nitrite reduction. Although the used POMs are generic ones, our methodology could be extended to many other new and exotic POMs. Due to the use of an ionic liquid containing a vinyl group, the incorporation of POMs in ionic liquid polymers (PILs)[43] that could be used for various electrocatalytic reactions[44] is readily envisaged.

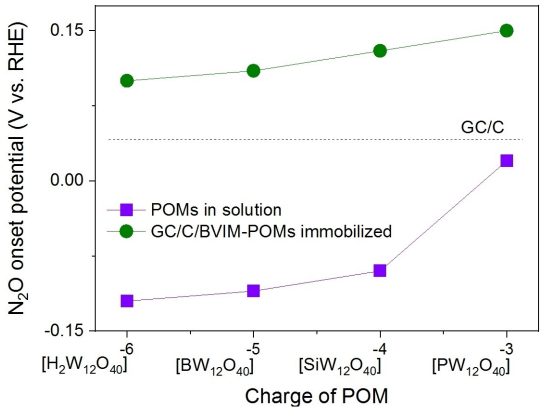

Figure 9. Comparison of onset potential of N_2O formation obtained with immobilized BVIM-POMs (this work) and our previous results obtained with POMs in solution.[11] The values are obtained from DEMS analysis.

Experimental Section

Reagents

All POMs used in this study were synthesized in our laboratory following well known protocols[45] except $(NH_4)_6[H_2W_{12}O_{40}]$ that was purchased from Sigma (Code 463922). Nafion solution (Code 274704), isotope ^{15}N labelled sodium nitrite (Code 364606) and sodium sulfate (Code 238597) were purchased from Sigma. Carbon black was purchased from Cabot (Code VXC72R) and glassy carbon electrode was purchased from Hiden Analytical. Ionic liquid 1-butyl-3-vinylimidazolium (BVIMBr) bromide (Code AB289818) was purchased from ABCR, Germany.

Preparation and Characterization of BVIM-POM Salts

An aqueous solution of POM was mixed with an aqueous solution of BVIMBr. The concentration of POM solution is 10 mM and the concentration of BVIMBr is prepared in such a way that the number of moles of $BVIM^+ = 2$*charge of POM*moles of POM. In this way an excess of BVIM is assured, assuming that the reaction is total (i.e. all the native cations of POM are replaced by $BVIM^+$, as proved by elemental analysis). A precipitation of a white salt is immediately observed. After vacuum filtration and multiple rinsing with distilled MiliQ (18 MΩ.cm) water, the salt is dried at room temperature overnight.

CHNS–O analyzer (FlashEA 1112 series) was used for elemental analysis. Infrared spectra were acquired with Jasco FT/IR-4600 device. TGA analysis were performed with Perkin analyzer in nitrogen atmosphere with a heating rate of 10 K/min and using aluminum oxide open crucibles. DSC analysis was performed with DSC 3 (Metler Toledo) in nitrogen atmosphere with a heating rate of 10 K/min and using 40 μL aluminum crucible with perforated lid. X-ray diffraction spectra have been acquired with a Bruker D8 Advance equipped with a non-monochromatic copper radiation (Kα = 0.154056 nm) and a Sol-X detector in the 20–70° 2θ range with a scan step of 0.016°.

^{31}P Solid-state MAS NMR experiments were performed at room temperature on an AVANCE 500 MHz wide bore spectrometer (Bruker™) operating at a frequency of 500.12 MHz for ^{1}H and 202.42 MHz for ^{31}P. Samples were spun at 22.5 kHz in a triple resonance $^{1}H/^{31}P/^{13}C$ MAS probe designed for 3.2 mm o.d. zirconia rotors closed with vespel caps. Details of data acquisition are given in the supporting information.

Preparation of GC/C/BVIM-POM Electrodes

The obtained BVIM-POM salt white powder is barely dispersed in water (10 mg/mL) using ultrasonic bath. In order to obtain an ink that could be cast on the electrode surface, carbon black is firstly dispersed in water (3 mg/mL) containing 10% Nafion. This suspension is mixed with BVIM-POM solution in a 1:2 v/v ratio. From this ink, 5 μL ink are dropped evenly on the surface of the glassy carbon electrode and dried in air. Then, extra 5 μL of stock Nafion solution are dropped on the electrode and dried in air. Then the electrode (GC/C/BVIM-POM) is ready for use. All four hybrid materials were used to obtain these electrodes. As some small amount of the hybrid material may not be strongly fixed on the electrode surface, cyclic voltammetry was run in clean electrolyte for several cycles until the curve is stable.

Electrochemical Characterization

Electrochemical studies were conducted in a classic three electrode cell with glassy carbon (3 mm diameter) as working electrode, Ag/AgCl (3 M KCl) as reference electrode and platinum wire as counter electrode, placed in a separated compartment by using a glass frit. Biologic SP300 potentiostat was used. All the solutions were degassed with an argon flow for 15 minutes und kept under Ar atmosphere. Glassy carbon was mechanically polished by using 6 μm, 3 μm and 1 μm diamond paste. The electrode was rinsed with distilled MiliQ (18 MΩ.cm) water and cleaned in an ultrasound bath. DEMS and classic electrochemical measurements were run in 0.5 M Na_2SO_4 pH 1 electrolyte containing only 10 mM $Na^{15}NO_2$. DEMS setup was described in our previous work and it is purchased from Hiden Analytical.[11] Briefly, the flow thin-layer electrochemical cell is composed of one glassy carbon rod as working electrode (5 mm diameter), Ag/AgCl (3 M KCl) as reference electrode and platinum wire as counter electrode, inserted in the outflow tube. A syringe pump assures the flow of the electrolyte at a speed of 0.5 mL/h. The distance between the surface of the working electrode and porous hydrophobic membrane is 1 mm. The total volume of the solution is 38 μL. The base pressure inside the mass spectrometer is $4*10^{-7}$ mTorr. The following m/z signals (m/z 31 for ^{15}NO, m/z 46 for $^{15}N_2O$ and m/z 30 for $^{15}N_2$) are recorded with a resolution of one measurement every 14 seconds.

Supporting Information

Supporting information is available.

Acknowledgements

Dr. Yulin Zhou acknowledges China Scholarship Council (CSC) for doctoral bursary. The authors acknowledge FRC Foundation (Frontier Research in Chemistry) as well as and the Labex Chemistry of Complex Systems for the purchase of DEMS. Authors also thanks the University of Strasbourg and the CNRS for constant financial support.

Conflict of Interests

The authors declare no conflict of interest.

Data Availability Statement

The data that support the findings of this study are available from the corresponding author upon reasonable request.

Keywords: DEMS · ionic liquid · immobilization · nitrite reduction · polyoxometalates

[1] M. Ammam, *J. Mater. Chem. A* **2013**, *1*, 6291–6312.
[2] A. Belhouari, B. Keita, L. Nadjo, R. Contant, *New J. Chem.* **1998**, *22*, 83–86.
[3] F. Boussema, R. Haddad, Y. Ghandour, M. S. Belkhiria, M. Holzinger, A. Maaref, S. Cosnier, *Electrochim. Acta* **2016**, *222*, 402–408.
[4] R. Naseer, S. S. Mal, U. Kortz, G. Armstrong, F. Laffir, C. Dickinson, M. Vagin, T. McCormac, *Electrochim. Acta* **2015**, *176*, 1248–1255.
[5] B. Wang, L. Cheng, S. Dong, *J. Electroanal. Chem.* **2001**, *516*, 17–22.
[6] L. Ruhlmann, G. Genet, *J. Electroanal. Chem.* **2004**, *568*, 315–321.
[7] S. Imar, M. Yaqub, C. Maccato, C. Dickinson, F. Laffir, M. Vagin, T. McCormac, *Electrochim. Acta* **2015**, *184*, 323–330.
[8] Y. Sahraoui, S. Chaliaa, A. Maaref, A. Haddad, N. Jaffrezic-Renault, *Journal of Sensor Technology* **2013**, *3*, 84–93.
[9] Y. Shan, G. Yang, Y. Sun, S. Pang, J. Gong, Z. Su, L. Qu, *Electrochim. Acta* **2007**, *53*, 569–574.
[10] Q. Wang, J. Khungwa, L. Li, Y. Liu, X. Wang, S. Wang, *J. Electroanal. Chem.* **2018**, *824*, 91–98.
[11] Y. Zhou, F. Bihl, A. Bonnefont, C. Boudon, L. Ruhlmann, V. Badets, *J. Catal.* **2022**, *405*, 212–223.
[12] A. Kondinski, *Polyoxometalates* **2024**, *3*, DOI: 10.26599/POM.2024.9140058.
[13] A. Barba-Bon, N. I. Gumerova, E. Tanuhadi, M. Ashjari, Y. Chen, A. Rompel, W. M. Nau, *Adv. Mater.* **2024**, *36*, 2309219.

[14] B. Khadro, I. Baroudi, A.-M. Goncalves, B. Berini, B. Pegot, F. Nouar, T. N. Ha Le, F. Ribot, C. Gervais, F. Carn, E. Cadot, C. Mousty, C. Simonnet-Jégat, N. Steunou, *J. Mater. Chem. A* **2014**, *2*, 9208–9220.
[15] B. Keita, A. Belhouari, L. Nadjo, R. Contant, *J. Electroanal. Chem.* **1995**, *381*, 243–250.
[16] S. Kakhki, E. Shams, M. M. Barsan, *J. Electroanal. Chem.* **2013**, *704*, 80–85.
[17] C.-J. Wang, S. Yao, Y.-Z. Chen, Z.-M. Zhang, E.-B. Wang, *RSC Adv.* **2016**, *6*, 99010–99015.
[18] Z. Zhang, X. Sun, H. Ma, H. Pang, S. Li, C. Zhao, *J. Mol. Struct.* **2016**, *1116*, 174–179.
[19] S. Li, H. Ma, H. Pang, L. Zhang, Z. Zhang, H. Lin, *Inorg. Chem. Commun.* **2014**, *44*, 15–19.
[20] P. Zhang, J. Peng, X. Shen, Z. Han, A. Tian, H. Pang, J. Sha, Y. Chen, M. Zhu, *J. Solid State Chem.* **2009**, *182*, 3399–3405.
[21] M. Ammam, J. Fransaer, *J. Solid State Chem.* **2011**, *184*, 818–824.
[22] F. M. Santos, S. P. Magina, H. I. S. Nogueira, A. M. V. Cavaleiro, *New J. Chem.* **2016**, *40*, 945–953.
[23] F.-C. Shen, Y.-R. Wang, S.-L. Li, J. Liu, L.-Z. Dong, T. Wei, Y.-C. Cui, X. L. Wu, Y. Xu, Y.-Q. Lan, *J. Mater. Chem. A* **2018**, *6*, 1743–1750.
[24] H. Liu, P. He, Z. Li, C. Sun, L. Shi, Y. Liu, G. Zhu, J. Li, *Electrochem. Commun.* **2005**, *7*, 1357–1363.
[25] B.-Q. Huang, L. Wang, K. Shi, Z.-X. Xie, L.-S. Zheng, *J. Electroanal. Chem.* **2008**, *615*, 19–24.
[26] R. Wang, D. Jia, Y. Cao, *Electrochim. Acta* **2012**, *72*, 101–107.
[27] S. Feizy, B. Haghighi, *J. Solid State Electrochem.* **2019**, *23*, 1339–1350.
[28] H. Ohno, *Macromol. Symp.* **2007**, *249–250*, 551–556.
[29] Q. Zhang, S. Wu, L. Zhang, J. Lu, F. Verproot, Y. Liu, Z. Xing, J. Li, X.-M. Song, *Biosens. Bioelectron.* **2011**, *26*, 2632–2637.
[30] Q. Zhang, X. Lv, Y. Qiao, L. Zhang, D.-L. Liu, W. Zhang, G.-X. Han, X.-M. Song, *Electroanalysis* **2010**, *22*, 1000–1004.
[31] A. Tézé, M. Michelon, G. Hervé, *Inorg. Chem.* **1997**, *36*, 505–509.
[32] I.-M. Mbomekallé, X. López, J. M. Poblet, F. Sécheresse, B. Keita, L. Nadjo, *Inorg. Chem.* **2010**, *49*, 7001–7006.
[33] D.-J. Guo, S.-J. Fu, W. Tan, Z.-D. Dai, *J. Mater. Chem.* **2010**, *20*, 10159–10168.
[34] M. S. Saraiva, J. A. F. Gamelas, A. P. Mendes de Sousa, B. M. Reis, J. L. Amaral, P. J. Ferreira, *Materials* **2010**, *3*, 201–215.
[35] Y. Ji, L. Shen, A. Wang, M. Wu, Y. Tang, Y. Chen, T. Lu, *J. Power Sources* **2014**, *260*, 82–88.
[36] E. J. Elzinga, D. L. Sparks, *J. Colloid Interface Sci.* **2007**, *308*, 53–70.
[37] M. S. Rayson, J. C. Mackie, E. M. Kennedy, B. Z. Dlugogorski, *Inorg. Chem.* **2012**, *51*, 2178–2185.
[38] C. Debiemme-Chouvy, H. Cachet, G. Folcher, C. Deslouis, *Electroanalysis* **2007**, *19*, 259–262.
[39] A. C. A. de Vooys, M. T. M. Koper, R. A. van Santen, J. A. R. van Veen, *J. Catal.* **2001**, *202*, 387–394.
[40] S. Heylen, S. Smeekens, C. Kirschhock, T. Parac-Vogt, J. A. Martens, *Energy Environ. Sci.* **2010**, *3*, 910.
[41] R. Wang, X. Zhang, Z. Ren, *J. Hazard. Mater.* **2021**, *402*, 123494.
[42] W. A. Brown, D. A. King, *J. Phys. Chem. B* **2000**, *104*, 2587–2595.
[43] J. Lu, F. Yan, J. Texter, *Prog. Polym. Sci.* **2009**, *34*, 431–448.
[44] Y. Zhang, Y. Li, H. Guo, Y. Guo, R. Song, *Mater. Chem. Front.* **2024**, *8*, 732–768.
[45] C. Rocchiccioli-Deltcheff, M. Fournier, R. Franck, R. Thouvenot, *Inorg. Chem.* **1983**, *22*, 207–216.
[46] T. Rajkumar, G. Ranga Rao, *Mater. Chem. Phys.* **2008**, *112*, 853–857.
[47] E. L. Hahn, *Phys. Rev.* **1950**, *80*, 580–594.
[48] S. Hediger, B. H. Meier, N. D. Kurur, G. Bodenhausen, R. R. Ernst, *Chem. Phys. Lett.* **1994**, *223*, 283–288.
[49] J. Raya, B. Perrone, J. Hirschinger, *J. Magn. Reson.* **2013**, *227*, 93–102.

Manuscript received: February 1, 2024
Revised manuscript received: May 31, 2024
Accepted manuscript online: June 12, 2024
Version of record online: ■■, ■■

RESEARCH ARTICLE

New hybrid materials were obtained by replacing innate cations of four Keggin-type polyoxometalates with an organic cation issued from an ionic liquid, 1-butyl-3-vinylimidazolium bromide. These materials show good activity towards nitric acid reduction after the immobilization on glassy carbon electrode. Differential electrochemistry mass spectrometry shows that overpotential of nitric oxide conversion to nitrous oxide is very much reduced.

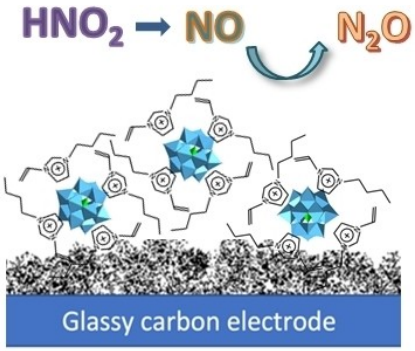

Dr. Y. Zhou, Dr. J. Sun, Dr. S. Gallet, Dr. J. Raya, Prof. C. Boudon, Prof. A. Bonnefont, Prof. L. Ruhlmann, Dr. V. Badets**